

## SiO<sub>2</sub>/Si<sub>3</sub>N<sub>4</sub>/Al<sub>2</sub>O<sub>3</sub> stacks for scaled-down memory devices: Effects of interfaces and thermal annealing

M. Lisiansky,<sup>a)</sup> A. Heiman, M. Kovler, A. Fenigstein, and Y. Roizin  
Tower Semiconductor Ltd., P.O. Box 619, Migdal HaEmek 23105, Israel

I. Levin  
Ceramics Division, National Institute of Standards and Technology, Gaithersburg, Maryland 20899

A. Gladkikh and M. Oksman  
Wolfson Applied Material Research Center, Tel Aviv University, Tel Aviv 69978, Israel

R. Edrei, A. Hoffman, and Y. Shnieder  
Department of Chemistry, Technion-Israel Institute of Technology, Haifa 32000, Israel

T. Claasen  
ASM Europe, Kapeldreef 75, 3001 Leuven, Belgium

(Received 23 March 2006; accepted 28 August 2006; published online 12 October 2006)

Effects of interfaces and thermal annealing on the electrical performance of the SiO<sub>2</sub>/Si<sub>3</sub>N<sub>4</sub>/Al<sub>2</sub>O<sub>3</sub> (ONA) stacks in nonvolatile memory devices were investigated. The results demonstrated the principal role of Si<sub>3</sub>N<sub>4</sub>/Al<sub>2</sub>O<sub>3</sub> and Al<sub>2</sub>O<sub>3</sub>/metal-gate interfaces in controlling charge retention properties of memory cells. Memory devices that employ both electron and hole trappings were fabricated using a controlled oxidation of nitride surface prior to the Al<sub>2</sub>O<sub>3</sub> growth, a high-temperature annealing of the ONA stack in the N<sub>2</sub>+O<sub>2</sub> atmosphere, and a metal gate electrode having a high work function (Pt). These devices exhibited electrical performance superior to that of their existing SiO<sub>2</sub>/Si<sub>3</sub>N<sub>4</sub>/SiO<sub>2</sub> analogs. © 2006 American Institute of Physics.  
[DOI: 10.1063/1.2360197]

Silicon-oxide-nitride-oxide-silicon (SONOS) memory and its nitride read only memory (NROM) modification are attractive solutions for future high-density data storage applications.<sup>1,2</sup> In these devices the information is stored as charges in the silicon nitride layer. In contrast to traditional SONOS memories, where program/erase operations involve direct electron tunneling through a thin (~20 Å) bottom oxide (BOX), in NROM these operations are accomplished by hot carriers (electrons/holes) locally injected over a barrier of a relatively thick (40–70 Å) oxide into the nitride layer near the drain.<sup>2,3</sup> As a result, 2 bits of information can be reliably stored in a single memory transistor.

Scaling down the SONOS memory cell to sub-100-nm technology nodes necessitates ONO stacks with small effective oxide thicknesses (EOTs). Currently, the only viable solution for achieving a sub-100-Å EOTs involves replacement of a conventional SiO<sub>2</sub> in the top dielectric layer with a material having higher dielectric constant (*k*). The high-*k* top layer is expected to provide several additional advantages including effective blocking of electron injection from the gate electrode and improved program/erase efficiency with a possibility of a Fowler-Nordheim (FN) hole injection from the substrate. The FN hole injection could provide an erase mechanism alternative to the currently used “hot” holes, which are the principal cause of the BOX degradation in NROM cells.<sup>3–5</sup> Moreover, the FN hole injection could enable a refresh operation of the memory cell.<sup>15</sup>

Aluminum oxide, Al<sub>2</sub>O<sub>3</sub>, (*k*=7–10) (Ref. 6) is regarded as one of the best candidates for the top oxide layer in ONO stacks due to its high thermal and chemical stabilities, electrical strength, and compatibility with conventional materials

used in the memory cell manufacturing.<sup>7–10</sup> Despite several promising results, a broad application of Al<sub>2</sub>O<sub>3</sub> in the SONOS memory stacks is hindered by several technical problems, including inferior retention characteristics compared to traditional NROM devices,<sup>8</sup> pinning effects at the Al<sub>2</sub>O<sub>3</sub>/poly-Si interface,<sup>9,11</sup> and mechanical stresses in Al<sub>2</sub>O<sub>3</sub> after the 900 °C annealing.<sup>12</sup>

The present letter reports a structural and electrical study of differently processed SiO<sub>2</sub>/Si<sub>3</sub>N<sub>4</sub>/Al<sub>2</sub>O<sub>3</sub> (ONA) stacks with a particular emphasis on the effects of (1) Si<sub>3</sub>N<sub>4</sub> surface preparation, (2) postdeposition annealing of the entire ONA stack, and (3) type of metal top electrode on the electrical characteristics of the resulting ONA-based memory devices.

The ONA stacks used in this study incorporated a dry grown SiO<sub>2</sub> layer (68 Å) and a Si<sub>3</sub>N<sub>4</sub> layer deposited by low-pressure chemical vapor deposition (CVD). The Al<sub>2</sub>O<sub>3</sub> layer (150 Å) was grown on top of the Si<sub>3</sub>N<sub>4</sub> layer using atomic layer CVD at *T*=450 °C. The Si<sub>3</sub>N<sub>4</sub> surface was used either as deposited (*A* type) or intentionally oxidized (about 10 Å deep) prior to the growth of Al<sub>2</sub>O<sub>3</sub> (*B* type).

The chemical structure of the alumina specimens was investigated by high-resolution transmission electron microscopy (HRTEM) and spatially resolved over the ONA thickness electron energy loss spectroscopy (EELS).<sup>13</sup>

Electrical characterization was performed using Si-ONA-metal (SONAM) capacitors with dimensions of 500×500 μm<sup>2</sup>. Prior to capacitor fabrication, the samples were annealed at 850 °C for 30 min in three different gas environments (O<sub>2</sub>, N<sub>2</sub>, and a N<sub>2</sub>+O<sub>2</sub> mixture).<sup>14</sup> Metal electrodes with large work function (Au and Pt) were used to increase the barrier height (~4 eV) for electron injection into Al<sub>2</sub>O<sub>3</sub>. The rear contact was fabricated using Al deposition.

<sup>a)</sup>Electronic mail: michaelx@towersemi.com

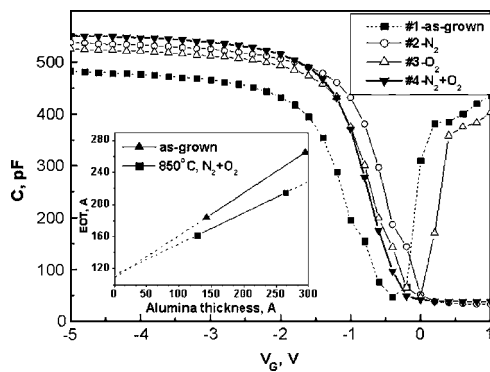


FIG. 1.  $C$ - $V$  characteristics ( $f=30$  Hz) of the  $A$ -type samples annealed in different gas environments. Similar effects were observed for the  $B$ -type stacks. An insert shows the EOT of the  $B$ -type stacks as a function of  $\text{Al}_2\text{O}_3$  thickness (150 and 300 Å) in the samples as deposited and annealed at 850 °C in the  $\text{N}_2+\text{O}_2$  mixture. The extrapolation to a zero thickness of  $\text{Al}_2\text{O}_3$  yields the effective EOT of the ON bilayer. A small increase of the bilayer EOT after annealing is observed.

Figure 1 shows the  $C$ - $V$  characteristics of the  $A$ -type samples before and after annealing in different gas environments. The annealing significantly reduced both the EOT and the positive charge in the stack (compare curves 1 and 2–4). The positive charge in the as-grown stacks was attributed to the  $\text{Si}_3\text{N}_4$  layer<sup>15</sup> and correlates with the reduction of the hydrogen content in this layer upon annealing.<sup>16</sup> The heat treatment in the  $\text{N}_2+\text{O}_2$  mixture yields the smallest EOT combined with a twofold reduction in the interfacial charges.

The  $I$ - $V$  characteristics of similar samples before and after annealing are summarized in Fig. 2. The annealing decreased the FN current “threshold” voltage, which is consistent with the observed reduction of the EOT. The gas environment has a pronounced effect on the leakage (subthreshold) currents. We argue that oxygen annealing reduces the number of oxygen vacancies and improves alumina stoichiometry, thereby reducing the trap-assisted currents.

Cross-sectional HRTEM/EELS studies of the as-grown samples confirmed the amorphous nature of  $\text{Al}_2\text{O}_3$  and revealed the presence of a partially oxidized nitride layer, hereafter denoted as SiON, at the  $\text{Al}_2\text{O}_3/\text{Si}_3\text{N}_4$  interface even in the  $A$ -type sample (Fig. 3). These results are consistent with a partial oxidation of the nitride surface upon exposure to air reported previously.<sup>16</sup> The oxidized layer in the  $A$ -type stack is nonuniform with the average thickness of less than 1 nm.

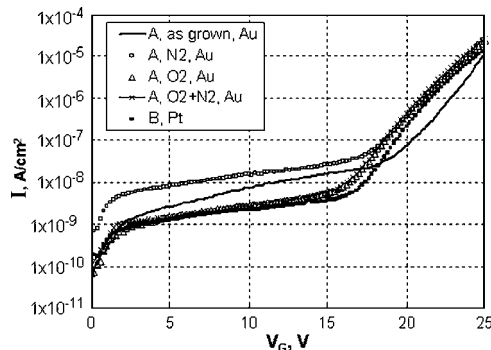


FIG. 2.  $I$ - $V$  characteristics of  $A$ -type samples (Au electrode): as grown and annealed at 850 °C in  $\text{N}_2$ ,  $\text{O}_2$ , and  $\text{N}_2+\text{O}_2$  mixture.  $I$ - $V$  curve for the  $B$ -type sample with the Pt electrode annealed at 850 °C in  $\text{N}_2+\text{O}_2$  is shown for comparison (Pt electrode is advantageous for blocking of electron injection at high currents).

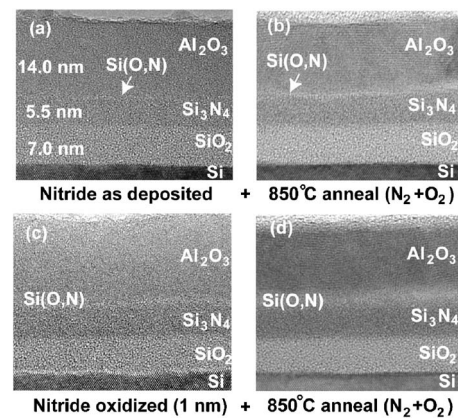


FIG. 3. HRTEM images of samples  $A$  [(a) and (b)] and  $B$  [(c) and (d)] before [(a) and (c)] and after [(b) and (d)] annealing at 850 °C in  $\text{N}_2+\text{O}_2$ . Crystallization of  $\text{Al}_2\text{O}_3$  and the evolution of the SiON interfacial layer are observed.

In contrast, controlled oxidation of the nitride surface in the  $B$ -type stacks generated a relatively uniform SiON layer of about 1 nm thick.

Annealing both  $A$ - and  $B$ -type stacks induced crystallization of  $\text{Al}_2\text{O}_3$ , regardless of the gas environment. Diffraction patterns and near-edge structure of the  $\text{Al}$ - $L_{2,3}$  and  $\text{O}$ - $K$  EELS edges (Fig. 4) all suggest a  $\gamma$ - $\text{Al}_2\text{O}_3$ -like polymorph as the crystalline phase.<sup>17</sup> A strong  $\langle 111 \rangle$  texture was observed. The crystallization was accompanied by about 10% reduction in the thickness of  $\text{Al}_2\text{O}_3$  layer, which is consistent with the 20% density increase commonly observed for the transformation from amorphous to  $\gamma$ -type  $\text{Al}_2\text{O}_3$ .<sup>18</sup>

In addition to crystallization of  $\text{Al}_2\text{O}_3$ , the annealing produced growth of the interfacial SiON layer. The resulting thickness of the SiON layer was about 2.5 nm in the  $B$ -type stack and about 1 nm in the  $A$ -type stack (annealing improved the uniformity of the SiON layer in the  $A$  type). The EELS suggested incorporation of Al into the SiON interfacial layer upon annealing, as evidenced by the characteristic change in the fine structure of the  $\text{Al}$ - $L_{2,3}$  edge on going from the crystalline  $\text{Al}_2\text{O}_3$  to the amorphous interfacial (Si,Al)ON layer (Fig. 4). Furthermore, the secondary ion mass spectroscopy revealed that the amount of hydrogen in  $\text{Al}_2\text{O}_3$  was reduced twice after the annealing. In parallel, the  $\text{Al}_2\text{O}_3$  dielectric constant increases from  $k \sim 7$  in the as-grown sample

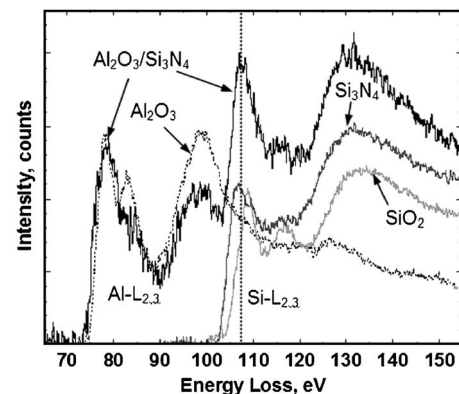


FIG. 4. Spatially resolved EELS spectra containing the  $\text{Al}$ - $L_{2,3}$  and  $\text{Si}$ - $L_{2,3}$  edges and recorded from the different layers in the  $B$ -type stack annealed at 850 °C in  $\text{N}_2+\text{O}_2$ . The spectra reveal clear changes in the near-edge structure of the  $\text{Al}$ - $L_{2,3}$  edge on going from  $\gamma$ -like  $\text{Al}_2\text{O}_3$  to the amorphous interfacial layer. These changes are consistent with Al being present in the amorphous interfacial layer.

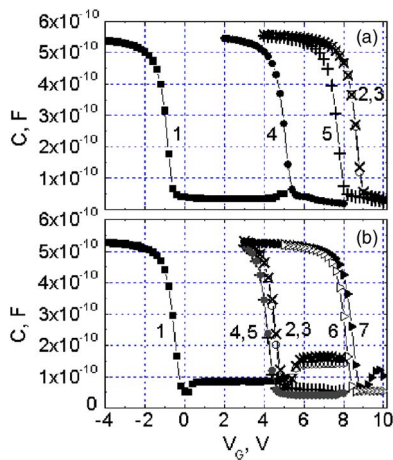


FIG. 5. (Color online) Charge loss effects observed in electron/hole-programmed capacitors (samples *A* and *B* annealed in  $N_2+O_2$ ). (a)  $C$ - $V$  curves for the *A*-type stacks with Au electrode: (1) initial; [(2) and (3)]  $e$  programmed (14 V) and biased positively and negatively, respectively, prior to the bake; and [(4) and (5)] biased positively and negatively, respectively, after the bake. (b)  $C$ - $V$  curves for the *A*- and *B*-type stacks with Pt electrode: (1) *A*-type initial; [(2) and (3)] *A*-type  $e$  programmed (14 V) and biased positively and negatively, respectively, prior to the bake; [(4) and (5)] *A*-type biased positively and negatively, respectively, after the bake; and [(6) and (7)] *B*-type  $e$  programmed (25 V) prior to and after the bake, respectively (program window  $\sim 9$  V,  $\Delta V_{fb} \sim 300$  mV).

to  $\sim 10$  (insert of Fig. 1). Thus, the reduction of EOT ( $\sim 10\%$ ) upon annealing can be attributed to crystallization of  $Al_2O_3$ . Extrapolation of the EOT dependence to the zero  $Al_2O_3$  thickness (Fig. 1) indicates that the EOT of a bilayer ON stack increases upon annealing. It can be ascribed to the growth of a SiON layer (Fig. 3) having the  $k$  value lower than that of the nitride.

Figure 5 presents results of a charge loss in capacitors based on the *A*- and *B*-type ONA stacks. The charging was performed using a FN injection from the substrate. Subsequent baking at  $150^\circ C$  for 1 h in the  $N_2$  atmosphere caused a significant loss of the trapped carriers. No correlation between the retention loss and the leakage current was observed. The best retention characteristics were obtained after annealing in the  $N_2+O_2$  mixture; however, the electron retention was still inferior to that of the standard NROM stacks ( $\Delta V_{fb} \sim 300$  mV for program window  $\sim 3$ – $3.5$  V). The origin of the retention loss in the electron/hole-programmed capacitors was determined by comparing standard baking and baking under a negative/positive voltage of 7 V applied to the gate. A complete suppression of charge loss when applying an appropriate voltage to the gate suggests that the loss occurs through the  $Al_2O_3$  layer.

For the  $Al_2O_3$ -controlled electron loss, any charges present in the vicinity of the  $Al_2O_3$ /metal-gate interface should either enhance (positive charges) or suppress (negative charges) the electron flow. This effect was confirmed using the  $C$ - $V$  test of the two capacitors. They were subjected to either positive or negative bias (5 V) which was applied to the gate electrode immediately prior to the bake. The electron loss in the capacitor having a positive charge at the  $Al_2O_3$ /Au interface was significantly higher than that in the capacitor with a negative charge [Fig. 5(a)]. A similar effect was observed for the hole-programmed capacitors. The effect of the interfacial charges is more pronounced for larger program windows. The effect of a prebake bias polarity was

much smaller for the Pt capacitors [Fig. 5(b)]. The hole-programmed Pt-gated capacitors demonstrated the largest program window of 5.5 V, which is consistent with the best blocking of electron injection into alumina. Thus, the interfacial charge is not an intrinsic property of  $Al_2O_3$  but is determined by the type of a metal electrode. Therefore, several other conventional materials having a high work function, such as TiN, TaN, and W, can be considered as potential candidates for a gate electrode.

Controlled oxidation of the nitride surface prior to  $Al_2O_3$  growth (*B*-type samples) significantly reduced the level of electron loss in the SONAM stacks. The *B*-type ONA structures demonstrated retention characteristics that were either very close or superior to the conventional ONO. For example, the sample with a Pt electrode annealed in the  $N_2+O_2$  mixture exhibited a retention loss of only 300 mV (for the 9 V program window) compared to 1 V in the *A*-type sample [see Figs. 5(a) and 5(b)]. This result suggests that a relatively thick (25 Å) interfacial (Si,Al)ON layer in the annealed *B*-type stack provides an efficient barrier for the electron escape into the metal electrode. We believe that the EOT of  $<100$  Å can be achieved for ONA stacks by further reduction of all layer thicknesses, thus enabling operating voltages below 6 V in NROM- and 10–12 V in SONOS ONA-based memory devices.

<sup>1</sup>B. Eitan, U.S. Patent No. 5,768,192 (16 June 1998).

<sup>2</sup>B. Eitan, P. Pavan, I. Bloom, E. Aloni, A. Frommer, and D. Finzi, *IEEE Electron Device Lett.* **21**, 543 (2000).

<sup>3</sup>Y. Roizin, E. Pikhay, and M. Gutman, *IEEE Electron Device Lett.* **26**, 35 (2005).

<sup>4</sup>R. Daniel, Y. Shaham-Diamant, and Y. Roizin, *Appl. Phys. Lett.* **85**, 6266 (2004).

<sup>5</sup>Y. Roizin, E. Pikhay, M. Lisiansky, A. Heiman, E. Alon, E. Aloni, and A. Fenigstein, *IEEE NVSMW 2006, Monterey, CA, 12–16 February 2006* (IEEE, New York, 2006), p. 74.

<sup>6</sup>G. D. Wilk, R. M. Wallace, and J. M. Antony, *J. Appl. Phys.* **89**, 5243 (2001).

<sup>7</sup>C. Lee, S. Hur, Y. Shin, J. Choi, D. Park, and K. Kim, *SSDM 2002* (unpublished), p. 162.

<sup>8</sup>M. Specht, H. Reisinger, M. Stadel, F. Hofman, A. Gschwander, E. Landgraf, R. J. Luyken, T. Schulz, J. Hartwich, L. Dreeskornfeld, W. Rosner, J. Kretz, and L. Rich, *33rd European Solid-State Device Research Conference, Estoril, Portugal, 16–18 September 2003* (IEEE, New York, 2003), p. 155.

<sup>9</sup>C. Lee, K. Choi, M. Cho, Y. Song, K. Park, and K. Kim, *Tech. Dig. - Int. Electron Devices Meet.* **2003**, 26.5.1.

<sup>10</sup>V. Gritsenko, K. Nayrov, Yu. Novikov, A. Aseev, S. Yoon, J. Lee, and C. Kim, *Solid-State Electron.* **47**, 1651 (2003).

<sup>11</sup>C. Hobbs, L. Fonseca, V. Dhandapani, S. Samavedan, B. Taylor, J. Grant, L. Dip, D. Triyoso, R. Hegde, D. Gilmer, R. Garcia, D. Roan, L. Lovejoy, R. Rai, L. Hebert, H. Tseng, B. White, and P. Tobin, *Tech. Dig. VLSI Symp.* **2003**, 9.

<sup>12</sup>T. Lee, C. Jang, B. Haselden, M. Dong, S. Park, L. Bartholomew, H. Chatham, and Y. Senzaki, *J. Vac. Sci. Technol. B* **22**, 2296 (2004).

<sup>13</sup>I. Levin, R. D. Leapman, M. Kovler, and Ya. Roizin, *Appl. Phys. Lett.* **83**, 1548 (2003).

<sup>14</sup>J. Lee, K. Koh, N. Lee, M. Cho, Y. Kim, J. Jeon, K. Cho, H. Shin, M. Kim, K. Fujihara, H. Kang, and J. Moon, *Tech. Dig. - Int. Electron Devices Meet.* **2000**, 645.

<sup>15</sup>M. Lisiansky, A. Heiman, G. Garteiz, E. Alon, A. Fenigstein, Y. Roizin, A. Gladkikh, M. Oksman, R. Edrei, A. Hoffman, G. Xing, and G. Cautiero, *Meet. Abstract, Electrochem. Soc.* **501**, 386 (2006).

<sup>16</sup>I. Levin, M. Kovler, Ya. Roizin, M. Vofsi, R. D. Leapman, G. Goodman, N. Kawada, and M. Funahashi, *J. Electrochem. Soc.* **151**, G833 (2004).

<sup>17</sup>A. Balzarotti, F. Antonangeli, R. Girlanda, and G. Martino, *Solid State Commun.* **44**, 275 (1982).

<sup>18</sup>I. Levin and D. Brandon, *J. Am. Ceram. Soc.* **81**, 995 (1998).